Estimating Flare Gas Heat Radiation Temperature and its Effect on FPSO Hull Corrosion in the Gulf of Guinea.

Charles, Watiminyo James[1], Izionworu, Vincent Onuegbu[2], Orji Charles U.[1] Wan Nik, W. M. N. B.[3] and James, Richard Victor[4]

1 Department of Marine Engineering, Faculty of Engineering, Rivers State University, Nkpolu-Oroworukwo, Port Harcourt, River State.
2 Department of Chemical/Petrochemical Engineering, Faculty of Engineering, Rivers State University, Nkpolu-Oroworukwo, Port Harcourt, River State.
3. Faculty of Ocean Engineering Technology and Informatics, Universiti Malaysia Terengganu, 21030 Kuala Nerus, Terengganu, Malaysia
4. Mechanical Engineering Department, University of Port Harcourt, Nigeria
Corresponding author's email: vincent.izionworu@ust.edu.ng; barawatiminyo@yahoo.com

ABSTRACT

Breakdown of Floating Production, Storage, and Offloading systems (FPSOs) due to corrosion has been a major cause of downtime in FPSO operating in various regions. A major cause of corrosion in the FPSO is the radiation from jet flame of gas flare stack installed on FPSO. Although gas flaring on the FPSO is very resourceful in the disposal of hydrocarbon gas resulting from a variety of process conditions it has become an "Achilles Heel". This study therefore sort to determine heat radiation from the gas flare stack in the Gulf Guinea on an FPSO and investigate the impact of the radiation on the Hull of the FPSO and other structures on it made of mild steel. The thermal radiation was simulated using PHAST - DNV software considering the production host peak period and off-peak period. The former period constitutes the harsh case the latter represents the mild case. A manual computation and conversion of the heat radiation from the FPSO was done and a temperature range of $T'_0 = 70°C$ and $T'_E = 96.2°C$ for mild case condition and $T'_O = 73.63°C$ and $T'_E = 118.4°C$ for worse case condition was determined. Gravimetric measurement was used to determine the weight loss from which the corrosion rate and metal loss were calculated. The influence of the resulting temperature as the major metocean condition of interest was determined and its synergistic interaction with other metocean conditions – pH and Salinity were examined. The results indicate that radiation from gas flare stack impacts on the corrosion rate and metal loss of mild steel used as a Hull for an FPSO in the Gulf of Guinea.

1.0   INTRODUCTION

All over the world, oil and gas exploration is faced with the challenge of fields in very deep water depths and uneconomical reserves with little or no profitable drive for exploitation by conventional fixed platform approaches (James, 2022). The choice and decision of the type of production process to be used are therefore dependent on a number of factors which amongst others include the Location of a Field and the size, its water depth, ocean currents, and how harsh the weather is. The best option for production purposes will hence not be a fixed installation following technical considerations given the challenges mentioned above. A floating unit would offer the best economic advantage (Pike, 1999). These

challenges necessitated the use of Floating Production, Storage, and Offloading systems (FPSOs) since the mid-1970s in offshore oil and gas production. FPSOs have proved to be quite beneficial and economical over fixed production platforms. This is especially when production is in remote deep-water locations or where it is difficult to install export pipelines and run them over time. The mobility of FPSOs is an amazing fit as they are floated off at the end of a field's productive life to another production field or location with great economic benefits such as a saved cost of facility fabrication, etc. This economic advantage is pronounced for marginal fields that have a short life span with production facilities required for only a few years (James, 2022).

Complex engineering drivers are usually engaged when a selection of an FPSO concept properly suited for specific field development is required. The need for FPSO has resulted to the common practice for oil tankers used for product delivery to be converted to an FPSO in the offshore oil and gas industry. A major driver of this initiative is the usually lower capital expenditure involved in the fabrication that converts a tank to an FPSO. Again, this possibility that has been exploited as was the case in the Gulf of Mexico (Ozgur, 2020) helps industry players to meet tight schedules. As a requirement some basic considerations are made during an oil tanker design, these design considerations such as speed, low fuel consumption, and carrying capacity are essentially what makes them suitable for conversion into FPSOs. The FPSO fatigue life left, that spent and the trading route are important factors (Ozgur, 2020; James, 2022). Tankers are designed to have large length/beam (L.B) ratios with comparatively slender hull forms to achieve speed and fuel economy,.

The design considerations of an FPSO implemented in the FPSO construction is such that they remain stationary at a location over a period bearing the designed storage capacity and yet support a large topside payload during downtime in production. The structural integrity of an FPSO hull usually has a weighty effect on both production plant, non productive time (NPT) and the mooring and riser systems. Any financial advantage associated with conversion of a tank to an FPSO or the outright construction of a new FPSO can be speedily lost if the FPSO hull design fails to address specific field environmental concerns embodied in the condition of the area. This kind of neglect in design leads to frequent shut-downs with the associated issues of loss of production or high cost of mooring and riser systems repairs. A crucial design consideration during the selection of the type of FPSO hull is the effect of the site-specific metocean conditions on the hull integrity and capacity to withstand degradation and failure of the coating system used on the hull to minimize production downtime resulting from damage of parent material of construction (James, 2022)

Materials selection during construction phases in FPSO projects, is based on the need to protect the hull from the hostile ocean environment. Some of these materials include marine Epoxy (Aluminum), marine Epoxy (Bronze), Epoxy Tie-Coat (Gray), slow polishing A-F (Red), etc. Any of the established methods could be used to select a suitable material to protect the hull if the ocean water temperature at the site is considered without any recourse to the additional temperature factor generated by the presence of the flare system installed on the FPSO deck. Other factors considered include climatic condition, diurnal and seasonal variations (Adrian *et al.,* 2004). A condition

that presents additional challenge is the artificial metocean condition created by the flare system on the main deck of any FPSO. The severity of this artificial condition depends on factors such as solar radiation, the pressure regime of the flare system, the condition of the flared gas (wet or dry), etc. This artificial ocean condition has the potential of damaging the hull faster than the traditional environment.

One major artificial metocean factor is the jet flame from gas flare stack on an FPSO. A jet flame occurs following the ignition and combustion of a flammable fluid issuing continuously from a pipe or orifice, which burns close to its release plane (Chamberlain, 1987). Releases of fuel jet fires could be accidental or intentional. A jet flame from flare systems of offshore oil and gas production facilities is an example of the latter. They offer a safe means of hydrocarbon gas resulting from a variety of process conditions disposal. Jet flames dissipate thermal radiation, which transmit heat energy that could be hazardous to life and property beyond the flames visible boundaries,. Thus, in the evaluation of the hazard posed by jet flames, the accurate determination of the likelihood of the amount of radiant energy received by objects at a distance from the flame is very important.

Three models namely Semi-empirical, Field, and Integral models have been developed to estimate the received radiated heat flux by objects at a distance from jet flames

Charles et al. (2022) stated that Semi-empirical models while predicting the shape of the flame and heat fluxes to external objects does not give details of the fire. They stated that this model subdivided into point source, multiple point source, and surface emitter models. Point source models represent the source of heat radiation by a point without a shape prediction (e.g., API-521 model). Multiple point source model mimics the effect of flame shape on radiated heat flux and gives the flame with a flame Centre line trajectory with numerous radiating point sources. They identified Surface emitter models flames as having the source of heat radiation from solid object like a cone or cylinder as. Field models are formulated on solutions of the time-averaged Navier-Stokes-equations for conservation of mass, momentum and other scalar quantities in a flowing fluid (Chamberlain, 1987). Sub-models are used to sufficiently describe important physical and chemical processes occurring in the combusting flowing fluid. They are complex computation with need for coding and noteworthy running time on higher computer configuration.

Integral models are go between semi-empirical and field models with simplified assumptions that help resolve resulting partial differential equations to ordinary differential equations and subsequently integrated. They are less rigorous and less computationally expensive when compared with Field models.

Semi-empirical models give best hazard assessment (Charles *et al.,* 2022). Compared to integral or field models, they are simpler to formulate, resolve mathematically and quicker write computer programs that run in shorter times. However, they depend heavily on empirical data, and specific to type of fire studied.

Chamberlain developed the surface emitter model extended by Johnson *et al.,* (2014). This model has been adopted and implemented in the JFSH model and forms the basis on which the Process Hazards Analysis Software Tool (PHAST) is founded.

The existing models indicate the need for empirical data to resolve site-specific metocean conditions at a particular location

since they influence the operability and availability of a spread-moored FPSO (Xia & Taghipour, 2012). In the design of the FPSO topsides and hull structures, as well as the design and selection of the process systems and equipment, designers must use site-specific metocean data. The hull and topsides systems and associated equipment are developed to project-specific FPSO motion criteria in an iterative manner, irrespective of all severe and unique metocean conditions. The difficulty associated with achieving a high availability target while meeting motion standards in the design of systems equipment and the hull design for a low-motion hull configuration calls for a multi-disciplinary approach with a realistic balance between expected hull motion and topsides availability with a focus on project-specific FPSO predicted performance despite severe specific metocean conditions (Xia, 2013).

The main design objectives for the operational metocean conditions should minimize the probability of vessel motion exceedance and the cumulative motion probability distributions for minimal structural, riser and mooring fatigue. Mooring systems have been affected by corrosion that exceeded the Classification or Class Societies corrosion allowance at the time at the range of 0.4 mm/y on each surface (Melchers et al, 2012). This challenge calls for the need to design having in mind metocean condition the FPSO will be exposed to, in respect to its natural periods of roll and heave which are determined from the field environmental data (Xia & Taghipour, 2012). Corrosion allowances of a 10-year service are provided for in different classification society standards like DNV Rules for ships (Adrian *et al.,* 2004) (Too short to be a paragraph)

However, while it is important to investigate the situation to find the best material to protect hulls of FPSO in the Gulf of Guinea, this study is an empirical one that focuses only on metocean conditions associated with thermal radiations from medium pressure (MP) and high pressure (HP) flare systems. It is therefore the objectives of this study to: (i) estimate the temperature of gas flare radiation in the Gulf of Guinea, (ii) estimate the impact of flare radiation temperature on the steel material used in the fabrication of the FPSO Hull and (iii) evaluate the synergetic effect of the interaction of temperature with other metocean parameters such as salinity and pH in a typical FPSO location like the Gulf of Guinea.

Investigation of other parts of the FPSO other than the hull with respect to the thermal radiation effect is not addressed in this work. This work will set the stage for empirical study of improved coating systems that will reduce the impact of FPSO hull corrosion.

2.0 MATERIALS AND METHODS
2.1 Materials
Materials used in this study include but are not limited to DNV Process Hazards Analysis Software Tool (PHAST) Software, Primary data - real process data from oil and gas facilities and data from FPSO. High energy filaments bulbs. Mild steel metal coupons machined to size 4 x 12 cm, density of 7.86 g/cm^3 and composed of C = 0.05%, Si = 0.03%, Mn = 0.6%, P = 0.35% and the remaining Fe%.

Four 100 liters drum. The Flare Stack Operating Parameter for Process Plant "E" and "O" selected for this research work is as presented in Tables 1 and 2 respectively.

2.2 Methods
There are basically two approaches to determining or sizing the flare stack of an FPSO. The first and simplest is the use of softbit flare simsoftware, the second method is manual sizing. The latter was chosen for the temperature

estimations because it offered the researchers the opportunity to estimate temperatures geo-thermally (geometry involving thermal radiations). The geometry associated with a typical gas disposal system is illustrated in Figure 1.

2.2.1 Estimating Flare Gas Thermal Radiation Temperature

Since every gas disposal system by combustion generates thermal radiation, the estimation of such thermal radiation involves multiple variables that involve numerous set of equations that make it practically impossible for manual estimations. Using
PHAST - DNV software the thermal radiation was simulated. The graphical results for two scenarios showing the relationship between thermal radiation-distance are presented in Figures 2 and 3.
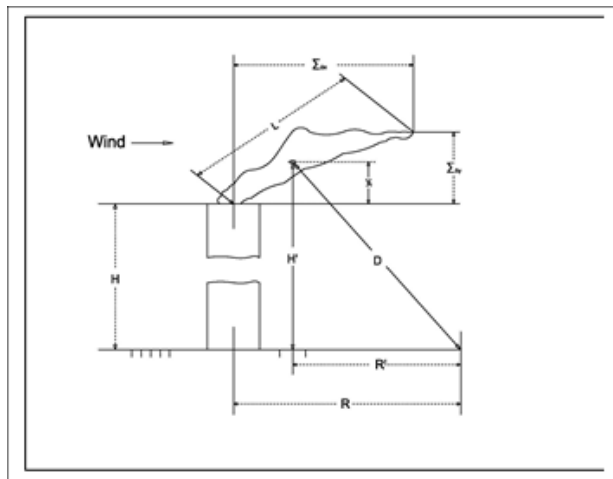

Figure 1: Geometry for flare stack manual sizing

In Figure 1; d = Diameter of flare stack; H = Height of flare stack;
D = Distance of receptor from flame centre; X_c = Flame centre horizontal distortion from flare stack centre; H^1 = Vertical height of distorted flame centre from flare stack base; Y_c = Vertical height of distorted flame centre from flare tip; L = Flame length; R^1 = Horizontal distance of flame centre to receptor; R = Horizontal distance of receptor

from flare stack base; $\sum \Delta x$ = Horizontal distance of distorted flame tip to stack centre; $\sum \Delta y$ = Vertical distance of distorted flame tip to flare stack tip.

2.2.2 Application of Geometry for Temperature Estimation

Figure 4 shows a typical sketch of a production host with a flare stack installed on the main deck. Practically speaking, the production host has peak period (when all oil storage tanks are full) and off-peak period when the crude oil has been evacuated by shuttle tankers. The former period constitutes the harsh case while the latter represents the mild case. The harsh case depicts a scenario where the freeboard of the production host is reduced due to volume of crude oil in the tanks. This in turn reduces the flare stack projection resulting in higher thermal radiation and temperature values on a receptor position on the sea surface proximate to the hull of the floater. The scenario is reversed for the milder case with resultant lower thermal radiation and temperature. The thermal radiations as well as the temperatures cannot be simulated accurately.

without considering the flare stack projection into the hull of the floater. Pythagoras theorem was employed to determine the distances of the receptor considering the effective flare stack height which is the sum of the stack height above the main deck plus the projected section. Figure 1 and 4 were combined to achieve the geometries representing the mild and harsh cases respectively. The dimensions of the geometric shapes were derived from the relevant flare stack height and width of the production host as Flare distance from Receptor at Off-Peak Period in the mild case, D'_o calculated from Pythagoras theorem as 68.5m, while the distance of the concerned receptor point for the flare stark 'D_E' is

calculated for Flare distance from Receptor at Off-Peak Period in the hash case, D'_E as 38.9m.

2.2.3 Temperature Estimations for FPSO Flare System Receptors

Thermal radiations temperature equivalents are determined either by mathematical correlations or simple thermal experiments. In this study mathematical correlations were used. The temperature estimation determined by sizing the flare stack can be based either on Softbit Flaresim software or manual sizing. Manual sizing was adopted because it offers researchers the opportunity to estimate temperatures geo-thermally (geometry involving thermal radiations).

Stefan-Boltzmann equation (1) used to calculate thermal radiation emitted by a body was not used in this study because the results were unrealistic This is likely due to the deviation of a conventional gas flare from the scenario modelled by the equation (1).

$$Q = \varepsilon \acute{O} A T^4 \qquad (1)$$

Accurate estimation of the temperatures was achieved by means of an experiment involving a 1kW electric filament and an industrial thermometer at standard atmospheric conditions. The results for eight hours shows that the filament emitted thermal radiation equivalent to 37°C.

The thermal radiations Q^1_S and Q^1_E corresponding to the distances D^1_0 and D^1_E for the mild case determined from Figures 2 & 3, are 1.945kw/m^2 and 2.6kw/m^2 respectively.

Also, from the thermal radiation emission experiment, the temperatures corresponding to these thermal radiation values by simple ratio are:

T'_0= 70°C and T'_E = 96.2°C for harsh condition and the thermal radiation values Q_O and Q_E corresponding to the distances D_O and

D_E for the Worse case are T_O = 73.63°C and T_E = 118.4°C

These temperatures are the temperatures associated with thermal radiations from flares of two flare starks installed in a production host on predetermined receptor point at 27m from the external hull. Table 3 gives the values of thermal radiation conversion to temperature selected for the experimental work. This was used to determine the effect of gas flare thermal radiation on the mild steel used for the fabrication of the FPSO.

2.2.4 Gravimetric Measurement

Manually calculated temperatures of T'_0= 70°C and T'_E = 96.2°C. were used to perform weight loss experimental measurement for four different artificial metocean conditions presented in Table 4. Four test drums/water baths were used for the experimental setup. Each test drum/water bath was maintained at conditions presented in Table 4 to simulate metocean condition with Gas flare from flare stack mounted 27 m away from the receptor; hence each of the baths are labelled Test Tank-1, Tank-2, Tank-3, and Tank-4 respectively. This is also depicted on the tags of the coupons as T-1, T-2, T-3, and T-4.

Table 3: Values of Thermal Radiation Conversion to Temperature Values

Flare Stacks	Thermal Radiation (kw/m^2)	Temp (°C)	Distance (m)
"O"	1.945	70	68.5
"E"	2.6	96.2	38.9

Raw research data

Table 1: Flare Stack Operating Parameter for Process Plant "E"

Flowrate (MMSCFD)	Gas	Inlet Pressure (bara)	Inlet Temperature (°C)	Flare Tip Diameter (inch.)	Flare Stack Height (m)
11.53	Methane	3.5	65	24	15

Table 2: Flare Stack Operating Parameter for Process Plant "O"

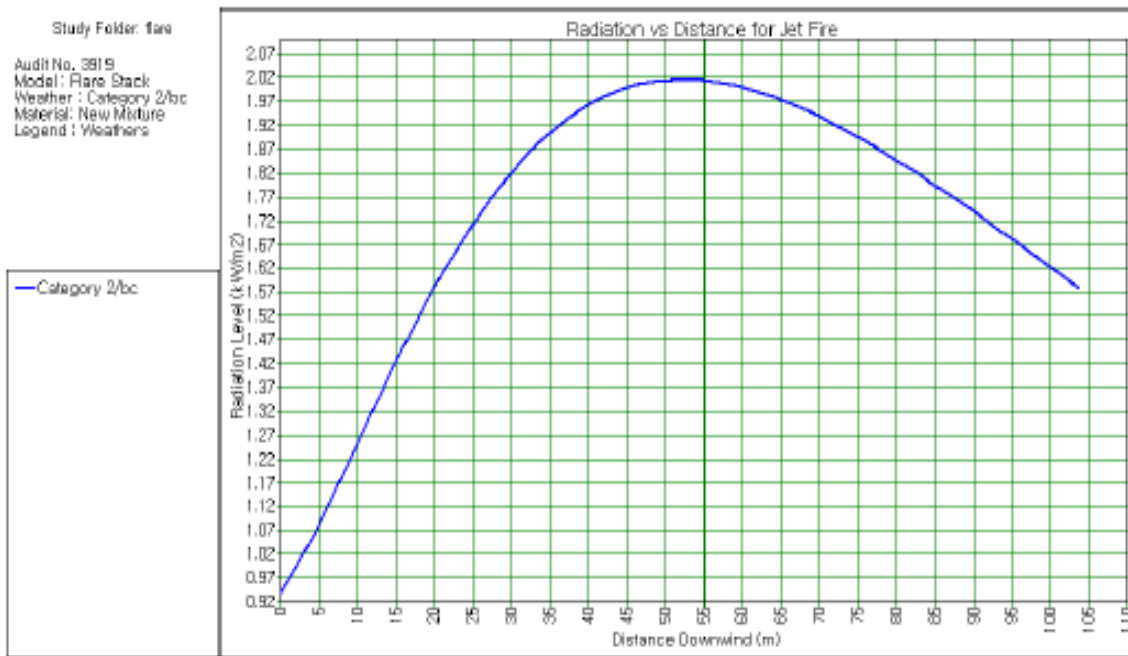| Flowrate (kg/hr)	Gas Data (%)	Inlet Pressure (Bar (a)	Inlet Temperature (°C)	Flare Tip Diameter (inch.)	Flare Stack Height (m)
288.664	N_2:0.12; CO_2:1.49 Methane: 87.09 Ethane:6.20; Propane:3.18 i-C4:0.73; n-C4:0.75 i-C5:0.07; n-C5:0.06	1.5	115	35	50

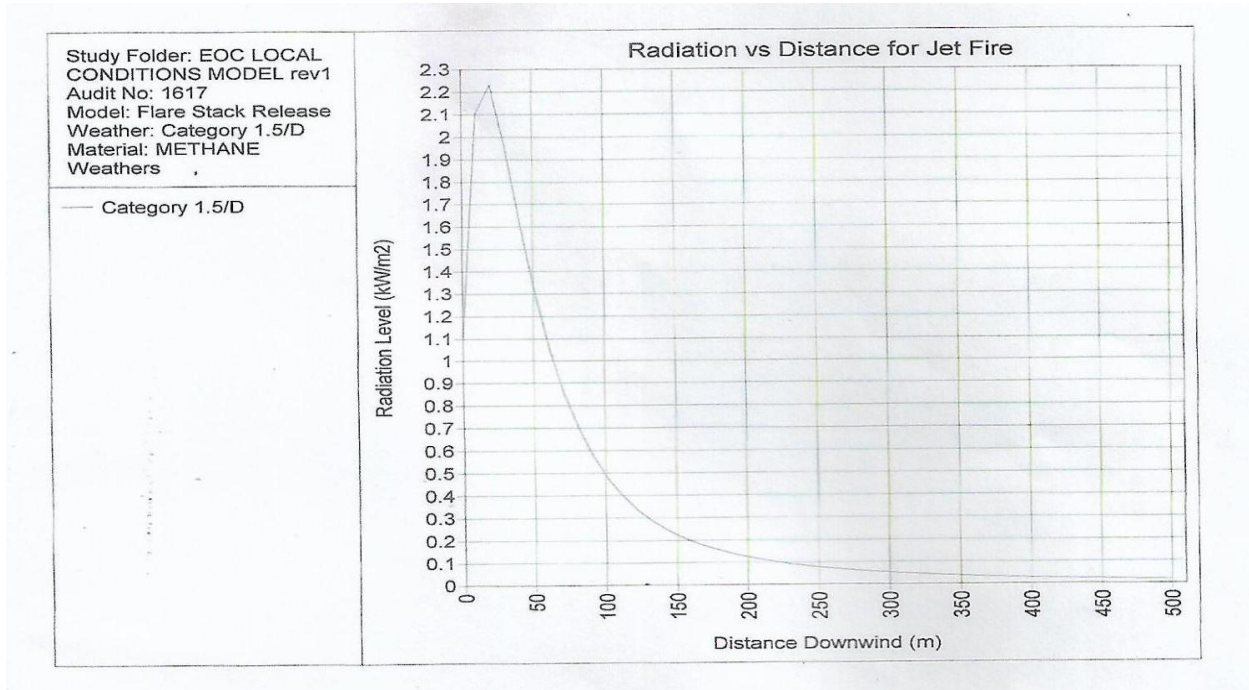**Figure 2: Thermal radiation distance graph for 2m/s for Flare stack "O"**

Figure 3: Thermal radiation distance graph for 21 m/wind velocity for stacks 'E'
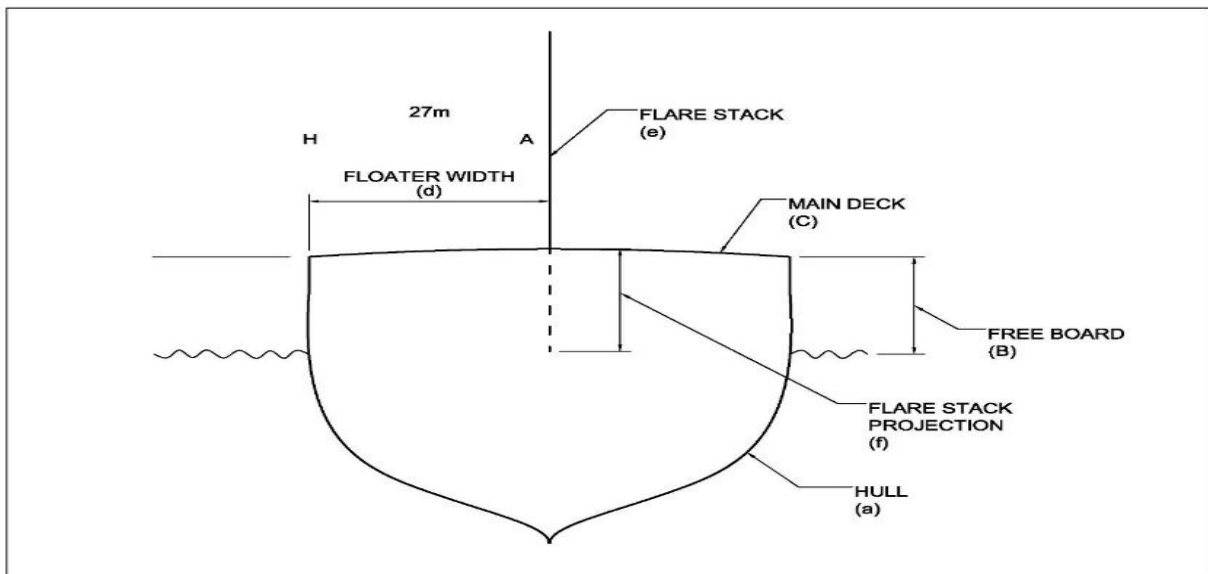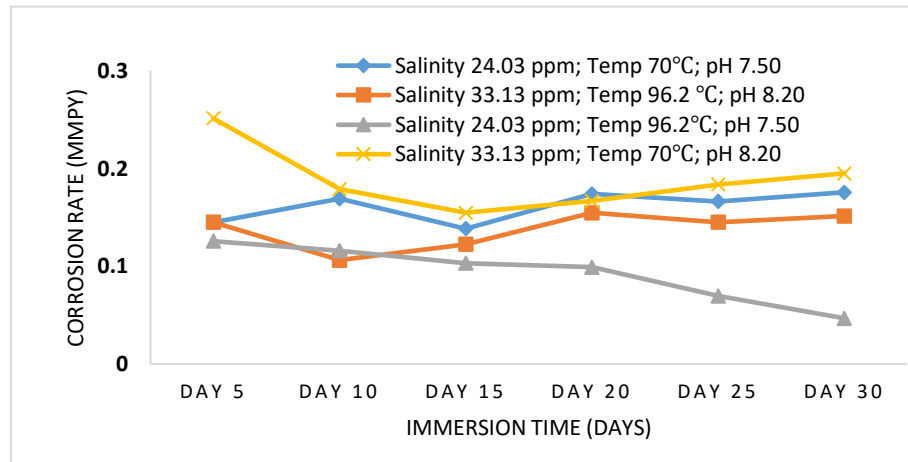

Figure 4: Production Host

Figure 5: Corrosion Rate of Mild Steel Coupons exposed to Artificial Metocean Conditions of Temperature 70°C and 96.2°C for 30 Days.

Blank mild Steel coupons were dipped into the simulated metocean condition of Table 4. The initial weights (W_o) of the mild steel coupon were obtain using an analytical weighing balance before their immersion in the test solutions of Salinity of 24.03 ppm; Temperature of 70°C and pH values of 7.50 represented as Tank 1; Salinity of 33.13 ppm; Temperature of 96.2°C and pH values of 8.20 represented as Tank 2; Salinity of 24.03 ppm; Temperature of 96.2°C and pH values of 7.50 represented as Tank 3 and the last simulated condition with Salinity of 33.13ppm; Temperature of 70°C and pH values of 8.20 represented as Tank 4.

Table 4: Simulated Metocean Condition

Tank	Artificial Metocean Parameters		
	Salinity (ppm)	Temp (°C)	Ph
1	24.03	70	7.50
2	33.13	96.2	8.20
3	24.03	96.2	7.50
4	33.13	70	8.20

Raw research data

After each of 5, 10, 15, 20, 25 and 30 days test period, the coupons were retrieved, washed under running water, followed by acetone, to remove any corrosion products. The cleaned coupons were then washed with distilled water, dried, and reweighed to determine their final weights (W_f). using equations 2 and 3 the results of gravimetric measurements were used

to calculate the corrosion rate (C_r), and metal loss (M_L) of the coupons in the simulated metocean condition.

$$C_r = \frac{W_L\,(8.75)(10^4)}{ADT} \qquad (2)$$

$$M_L = \frac{W_L\,10}{DT} \qquad (3)$$

Where WL is the weight loss of the mild steel, A is the area of the coupon, D is total surface area of the mild steel, T is the test duration in hours.

3.0   RESULTS AND DISCUSSION

3.1   Results of Estimating Flared Gas Heat Radiation Temperatures

The manual flare stark sizing methodology discussed in section 2.2.1 to 2.2.3 were used to estimate the temperatures associated with thermal radiations involving hydrocarbon gas flare Stark installed in a production host with respect to predetermined receptor point at 27m on external hull. The distance of the flared gas radiation from the receptor was manually calculated to be D_o = 61.5m and 38.8m representing two cases (harsh or worst and mild). After mathematical analysis, the temperatures for the mild case were found to be 70 °C and 96.2 °C while the harsh case has 73.63°C and 118.4 °C. For the purpose of this work and limitations in materials, the mild case parameters were used to test the effect of flare stack thermal radiation on the FPSO it is mounted on. Artificial metocean conditions in Tank were simulated and sustained during the period at temperatures of 70 °C and 96.2 °C. The high temperature hydrocarbon gas flare condition was simulated with, three high energy filament bulbs were used resulting to 96.2°C. The low temperature condition was simulated using two high energy filament bulbs resulting to 70 °C.

3.2 Results of Corrosion Induced by Estimated Flared Gas Heat Radiation Temperatures on FPSO Fabricated with Mild Steel.

The corrosion effect of the estimated flared gas heat radiation temperature on the FPSO is determined using gravimetric or weight loss measurements described in section 2.2.4 and presented graphically in Figure 5. The result indicates that mid steel coupon in Tank 4, which had high pH, high salinity, and low temperature had the most weight loss. Coupons in Tank 1 and 2 were the next in rank in weight loss. Coupons in Tank 3 had the least weight loss.

The influence of low salinity, low temperature, and low pH on the mild steel coupons exposed in Tank 1 indicates a corrosion rate that fluctuates slightly over time but remains relatively
moderate compared to other tanks as seen in the plot of Figure 5. The fluctuation might be due to varying Temperature (Gómez-Sánchez *et al*., 2023; Izionworu et al., 2020b; Agi *et al*., 2018) and other environmental factors or changes in the metal's surface condition with a possibility of passivity of the metal. Researchers have identified this trend as a common trend when mild steel which forms a passive film on its surface (Izionworu *et al.,* 2020; Han, 2009).

Tank 2 exhibits a corrosion rate that initially starts moderate but decreases over time with high salinity, high temperature, and high pH. This could be due to the formation of

protective layers on the metal surface or a decrease in the aggressiveness of the corrosive environment due to the effect of temperature on the salt component of the simulated sea water (Wang *et al.,* 2019; Lokas & Alar 2019). The plot for Tank 3 which has low salinity but high temperature and low pH exhibits a relatively high corrosion rate, especially in the later stages of the observation period. It is instructive that despite the low salinity, the combination of high temperature and low pH leads to a relatively high corrosion rate, especially. This experience is understandable as the temperature has been reported to increase the rate of corrosion (Gómez-Sánchez *et al.,* 2023; Izionworu *et al.,* 2020a; Izionworu *et al.,* 2020b, Agi *et al.,* 2018), and in some cases where every other factor remains constant by 10% (Adrien *et al.,* 2004)

However, the corrosion rate in Tank 4 is consistently high throughout the observation period, indicating that the combination of high salinity and high pH contributes significantly to the corrosion of mild steel.

Tanks with high salinity (Tanks 2 and 4) generally show higher corrosion rates compared to tanks with low salinity (Tanks 1 and 3). This is in agreement with published research evidence in industry experience that salinity plays a significant role in accelerating corrosion which is why offshores structures like FPSO's require protective coatings (Bai *et al.,* 2022). The influence of the radiation from the gas flare on the Flare Stack are seen in Tanks 2 and 3 where corrosion rate is higher. While the effect of pH is less clear-cut but seems to interact with other factors. Tanks 2 and 4, which have high pH, exhibit high corrosion rates, while Tank 3, with low pH,

also shows relatively high corrosion rates, especially at higher temperatures.

In Figure 6 the metal loss in Tank 1 is seen to be relatively consistent over the observation period, with slight fluctuations but no clear trend. Despite the low salinity, temperature, and pH, the metal loss is not significantly lower compared to other tanks.

Tank 3, indicating that high salinity and pH play significant roles in accelerating corrosion. Tanks with high salinity (Tanks 2 and 4).

In Figure 6 it is also observed that Tank 2 exhibits a consistent pattern of metal loss, with a slight decrease observed around Day 10 before increasing again towards Day 30. Despite the harsher environmental conditions with high salinity, temperature, and pH, the metal loss remains relatively comparable to Tank 1. A gradual decrease in metal loss over the observation period, with a significant reduction by Day 30 in Tank 3. Despite the high temperature, the metal loss is lower compared to Tank 2 and similar to Tank 1, indicating that low salinity and pH resulted in lower corrosion. However, Tank 4 exhibits fluctuations in metal loss, with peaks around Day 20 before decreasing again by Day 30.Despite the reported low temperature, the metal loss is higher compared to Tank 1 and generally exhibit higher metal loss compared to tanks with low salinity (Tanks 1 and 3), Although Sani *et al.,* (2019) reported decrease in corrosion with increase in salinity this experience agrees with other previous researchers that reported increase in corrosion of mild steel with increase in salt concentration of an electrolyte (Sondjono, 2017). Sondjono *et al.,* explained that chloride ion affects the corrosion rate (Bai *et al.,* 2022). This however

explains why an FPSO in Gulf of Guinea with high salinity suffer significantly from corrosion. Although the plots show that temperature and pH variations do not show a straight forward correlation with metal loss, as evidenced by the mixed results across tanks, it is noteworthy that temperature influences corrosion as has been reported and may likely be the reason for increase in metal loss with increased insalinity. The complicated prediction of metal loss resulting from the interaction of multiple parameters highlights the importance of considering all environmental factors in corrosion studies.

4.0 CONCLUSION

The temperature of gas flare radiation on typical FPSO in the Gulf of Guinea has been estimated to be 70°C for mild case condition and 96.2^{o}C for the harsh condition using manual calculation. The effect of these temperatures in the two conditions on an FPSO

has also been demonstrated. The result indicate that the temperature of the metocean condition affected the mild steel corrosion leading to an increase in the corrosion rate. Other parameters such as salinity, and pH also play a role in determining the corrosion rate of mild steel used in the FPSO fabrication. The interaction of temperature and these parameters can be complex. Higher temperature in a mix with higher salinity, and higher pH generally lead to higher corrosion rates, but the specific effects can vary depending on the combination of parameters as demonstrated in the study.

Again, while salinity appears to have a significant influence on metal loss, the effects of temperature and pH are more nuanced and may vary depending on other environmental factors. This indicates that jet flame impacts the metal structures of FPSO's.
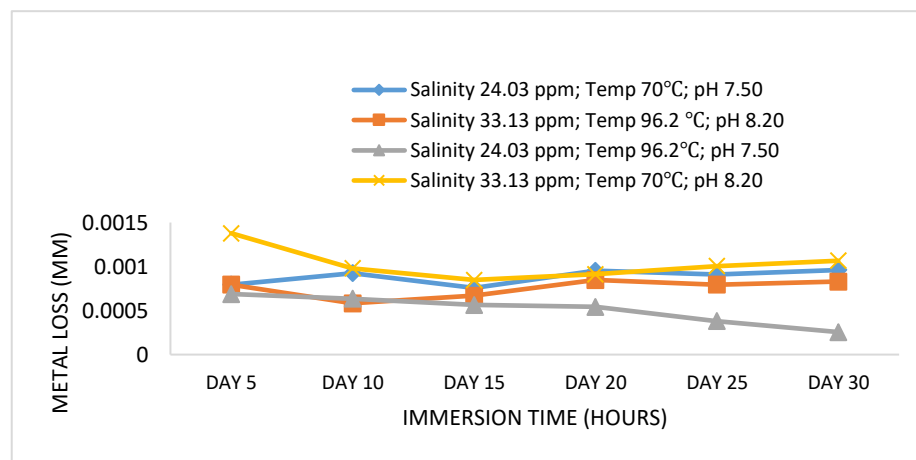

Figure 6: Metal Loss of Mild Steel Coupons exposed to 70°C and 96.2°C Different Artificial Metocean Temperature Conditions for 30 Day

Therefore, there is need to develop a suitable corrosion control coating system that will resist the consequential heat effect that leads to, or increases the rate of corrosion of an FPSO. Investigation and analysis of the effect of temperature from gas flare, and the synergistic effects of salinity and pH conditions to understand the complex interplay of these parameters in corrosion processes and mitigating corrosion in practical applications would be recommended for any coating system used as a corrosion preventive measure for structures exposed to these metocean conditions.

5.0 ACKNOWLEDGMENTS

REFERENCES

Adrien, M., Karl, P.F., Henning, C., Oystem, G. & Det, N.V. (2004). Newbuild FPSO Corrosion Protection – A design and Operation Planning Guideline. Prepared for *Offshore Technology Conference*, 1-11.

Agi, A., Junin, R., Zakariah, M. I., & Bukkapattanam, T. B. (2018). Effect of temperature and acid concentration on Rhizophora mucronata tannin as a corrosion inhibitor. *Journal of Bio-and Tribo-Corrosion,* 4, 1-10.

Anomohanran, O. (2015). Evaluating the Thermal Impact of Gas Flaring in Kokori, Southern Nigeria. *Applied Physics Research*, 7(1), 78-83.

Aromaa, J., Ronkainen, H., Mahiout, A., & Hannula, S. P. (1991). Identification of factors affecting the aqueous corrosion properties of (Ti, Al) N-coated steel. *Surface and Coatings Technology*, 49(1-3), 353-358.

Bai, X., He, B., Han, P., Xie, R., Sun, F., Chen, Z., ... & Liu, X. (2022). Corrosion behavior and mechanism of X80 steel in silty soil under the combined effect of salt and temperature. *RSC advances*, *12*(1), 129-147.

Chamberlain, G.A. (1987) Developments in Design Methods for Predicting Thermal Radiation from Flares. *Chemical Engineering Resources, Pes*. 65, 299-310.

Charles, W. J., Izionworu, V. O. Orji, C. U. (2022). FPSO Hull Corrosion Management to Minimize Operational Down-Time Due to Artificial Metocean Conditions: A Thermal Approach. *Proceedings of the International Conference on Newviews in Engineering and Technology* (ICNET) Maiden Edition, Faculty of Engineering, Rivers State University, Port Harcourt, Nigeria.

Smith, C. (2005). Coatings for Corrosion Protection: Offshore Oil and Gas

Operation Facilities, Marine Pipeline and Ship Structures" (2004). *US Department of Commerce, Technology Administration, National Institute of Standards and Technology.*. 1035 (1), 6.

Daniel-Mkpume, C. C. Ani, A. C., Okonkwo, G. E. Offor, P. O., Iloanusi, O.N., Egoigwe, V. & Abraham O. F. The Effect of Temperature on Corrosion Inhibition of a Blend of African Star Apple Seed Extract on Mild Steel Immersed in HCl Solution. *1st International Multidisciplinary Conference on Technologyk* 110-117.

Farag A. A., Ismail, A. S., & Migahed, M. A. (2015). Inhibition of Carbon Steel Corrosion in Acidic Solution Using Some Newly Polyester Derivative. *Journal of Molecular Liquids* 211, 915-923.

Gómez-Sánchez, G, Olivares-Xometl, O, Arellanes-Lozada, P, Likhanova, N.V., Lijanova, I.V,, Arriola-Morales, J, Díaz-Jiménez, V, López-Rodríguez, J. (2023). Temperature Effect on the Corrosion Inhibition of Carbon Steel by Polymeric Ionic Liquids in Acid Medium. *International Journal of Molecular Sciences.*; 24(7), 6291.

Han, J., Young, D., Colijn, H., Tripathi, A., & Nešić, S. (2009). Chemistry and structure of the passive film on mild steel in CO2 corrosion environments. *Industrial &* *Engineering Chemistry Research*, *48*(13), 6296-6302.

Izionworu, V. O., Oguzie, E. E. & Amadi, S. A. (2020). Electrochemical, SEM, GC-MS And FTIR Study Of Inhibitory Property of Cold Extract of Theobroma Cacao Pods For Mild Steel Corrosion In Hydrochloric Acid. *International Journal of Engineering Trends and Technology* 68(2), 82-87.

Izionworu, V.O., Ukpaka, C.P. & Oguzie, E.E. (2020a). Inhibition Of Mild Steel Corrosion In Acidic Medium Using Theobroma Cacao Pod. *International Journal of Scientific & Engineering Research*, (11)3, 255-256.

Izionworu, V.O., Oguzie, E.E. & Arukalam, O.I. (2020b). Thermodynamic and Adsorption Evaluation of Codiaeum Variegatum Brilliantissima - Zanzibar as Inhibitor of Mild Steel Corrosion in 1 M HCl. *Journal of Newviews in Engineering and Technology*, 2(4), 1-13.

Izionworu, V.O, Puyate, Y.T. & Wan-Nik, W. M.N. (2021). A Study of Wire Croton as an Inhibitor of Mild Steel in HCL Using Electrochemical – SEM – GCMS and FTIR Measurements. *Journal of Newviews in Engineering and Technology*, 3(1), 1-11.

Izionworu, V. O., Byadi, S., Arukalam, I. O., & Nik, W. M. N. W. (2022). Inhibitive Mechanism of Acid Corrosion of Cold-Rolled Steel by Polyethylene Glycol via Experimental,

Computational and Surface Analytical Approaches. *Journal of Bio-and Tribo-Corrosion*, 8(14), 14.

James C. (2022). Floating Production Storage and Offloading (FPSO) Overview. *Investipedia, 1(6), 1-3.*

Johnson A.D., Brightwell H.M. & Carsley A.J. (2014). A Model For Predicting The Thermal Radiation Hazards From Large-Scale Horizontally Released Natural Gas Jet Fires. Shell Research Ltd., Thornton Research Centre, Chester CHI 3SH,123 – 142

Lokas L., & Alar, V. (2019). The effect of temperature on corrosion behavior of AA5083 in brackish water and seawater. *Materials and Corrosion*, *70*(10), 1817-1825.

Melchers, R.E., Jeffery, R. & Fontaine, E. (2012). Corrosion and the structural safety of FPSO Mooring Systems in Topical Waters. *Proceedings of the OTC*.

NIOSH [2016]. NIOSH Criteria for a Recommended Standard: Occupational Exposure to Heat and Hot Environments. U.S. Department of Health and Human Services, Centers for Disease Control and Prevention. *National Institute for Occupational Safety and Health*, DHHS (NIOSH) Publication 1 - 192.

Oguzie, E. E. (2007). Corrosion inhibition of aluminum in acidic and alkaline media by Sansevieria trifasciata extracts. *Corrosion Science, 49*, 1527-1539.

.

Oguzie, E. E., Enenebeaku, C. K., Akalezi, C. O., Okoro, S. C., Ayuk, A. A., & Ejike, E. N. (2010). Adsorption and Corrosion inhibiting effect of Dacryodis edulis extract on low carbon steel corrosion in acidic media. *Journal of Colloid Interface Science, 349*(283).

Ozgur O., (2021). Conversion of an oil tanker into FPSO in Gulf of Mexico: strength and fatigue assessment, Ships and Offshore Structures. *Ships and Offshore Structures*,16(9), 993-1011.

Pike, W.J. (1999). Economic Benefits of FPSO Construction and Deployment in the Gulf of Mexico. *Offshore Technology Conference,* Houston, Texasdoi.

Ramesh, S. (2014). Corrosion Control for Offshore Structures. (1ˢᵗ ed). Waltham, MA 02451, USA. *Elsevier Inc*.

Ramesh, S. P., Vinod Kumar, K. P., & Sethuraman, M. G., (2001). Extract of *andrographis paniculata* as corrosion inhibitor of mild steel in acid medium, *Bulletin of Electrochemistry*, 17, 141–144.

Sani, F. M., Brown, B., Belarbi, Z., & Nesic, S. (2019). An experimental investigation on the effect of salt concentration on uniform CO2 corrosion. *In Nace Corrosion*, 13026.

Shylesha, B. S., Venkatesha, T. V., & Praveen, B. M. (2011). Corrosion inhibition

studies of mild steel by new inhibitor in different corrosive medium. *Research Journal of Chemical Sciences*, 1(7), 46-50.

Sundjono, S., Priyotomo, G., Nuraini, L., & Prifiharni, S. (2018). Corrosion Behavior of Mild Steel in Seawater from Northern Coast of Java and Southern Coast of Bali, Indonesia. *Journal of Engineering and Technological Sciences*, 49(6),

Yadav, M., Sinha, R. R., Sarkar, T. K., Bahadur, I., & Ebenso, E. E. (2015). Application of New Isonicotinamides as a Corrosion Inhibitor on Mild Steel in Acidic Medium: Electrochemical, SEM, EDX, AFM and DFT investigations. *Journal of Molecular Liquids*. 212, 686-698.

Xia, J. (2013). FPSO Design to Minimise Operational Downtime due to Adverse Metocean Conditions off North West Australia. *Deep Offshore Technology,* 27-29. Perth, Australia.

Xia, J., & Taghipour, R. (2012). Feasibility of TLP with tender assisted drilling for northwest Australian waters-A case study. In *Offshore Technology Conference* (OTC), 23247.

Wang, L., Gao, Z., Liu, Y., Lu, X., Wang, C., & Hu, W. (2019). Effect of temperature on corrosion behavior of X65 steel in simulated deep sea environment. *International Journal of*

Electrochemical Science, *14*(1), 161-172.